

# A 3-D Pseudo-Arc-Length Method for Numerical Simulation of Detonation Wave Propagation

Tianbao Ma, Jinqing Zhao, Jianguo Ning\*  
State Key Laboratory of Explosion Science and Technology,  
Beijing Institute of Technology, Beijing, People's Republic of China

## 1 Introduction

Detonation is a chemical reaction transmission process with a large amount of energy release. It involves complex interaction between reactive chemical kinetics and fluid dynamics. Numerical simulation of the detonation wave propagation is an important research field and many references can be found in the literature [1, 2]. How to accurately capture and track the propagation of shock wave is always a difficult problem in detonation simulations. One of the conventional methods is to increase the number of computational grids. However, as the number of grid cells increases, the computational complexity increases rapidly. Therefore, to capture the detonation wave with high accuracy and keeping the computational cost within acceptable limits are major challenges. In order to achieve this, mesh adaptation is an essential tool for solving such problems.

Many studies have investigated moving mesh methods applied to singularity problems for one- and two-dimensional hyperbolic equations. However, the extension of moving mesh methods to three-dimensional computation is always non-trivial. The most difficult aspects of three-dimensional computation are mesh redistribution and physical interpolation redistribution on a new mesh. An important intuitive approach for determining the mesh point relocation and movement is to minimize some functional formulated to measure the error or difficulty in numerical simulation.

The objective of the present study is to present a robust, stable, and effective three-dimensional scheme for detonation wave propagation. We propose an arc-length moving mesh scheme to deal with the strong discontinuity of detonation wave propagation in three-dimensions, similar to the arc-length methods used in the singularity behaviors problem. Further, we present a numerical example to compare our results with those presented in [8, 9] in order to prove that our scheme is stable and reliable.

## 2 Governing equations

The governing equations which describe the flow and reaction evolution with a single step chemical reaction model:

$$\frac{\partial \mathbf{w}}{\partial t} + \frac{\mathbf{f}(\mathbf{w})}{\partial x} + \frac{\mathbf{g}(\mathbf{w})}{\partial y} + \frac{\mathbf{h}(\mathbf{w})}{\partial z} = \mathbf{s}(\mathbf{w}), \quad (1)$$

where the conserved variable vector  $\mathbf{w}$ , the flux vectors  $\mathbf{f}(\mathbf{w})$ ,  $\mathbf{g}(\mathbf{w})$ , and  $\mathbf{h}(\mathbf{w})$ , and the source vector  $\mathbf{s}(\mathbf{w})$  are given:

$$\mathbf{w} = (\rho, \rho u, \rho v, \rho w, E, \rho Y)^T \quad (2)$$

$$\mathbf{f}(\mathbf{w}) = (\rho u, \rho u^2 + p, \rho uv, \rho uw, (E + p)u, \rho u Y)^T \quad (3)$$

$$\mathbf{g}(\mathbf{w}) = (\rho v, \rho uv, \rho v^2 + p, \rho vw, (E + p)v, \rho v Y)^T \quad (4)$$

$$\mathbf{h}(\mathbf{w}) = (\rho w, \rho uw, \rho vw, \rho w^2 + p, (E + p)w, \rho w Y)^T \quad (5)$$

$$\mathbf{s}(\mathbf{w}) = (0, 0, 0, 0, 0, \dot{\omega})^T \quad (6)$$

Here  $u$ ,  $v$ , and  $w$  are the Cartesian components of the fluid velocity in the  $x$ ,  $y$ , and  $z$  directions, respectively,  $\rho$  is the density,  $p$  is the pressure,  $E$  is the total energy per unit volume, and  $Y$  is the reactant mass fraction. The total energy  $E$  is defined by

$$E = \frac{p}{\gamma - 1} + \frac{1}{2}\rho(u^2 + v^2 + w^2) + \rho QY, \quad (7)$$

where  $Q$  is the heat released by the reaction and  $\gamma$  is the specific heat ratio. The source term  $\dot{\omega}$  is assumed to be in an Arrhenius form

$$\dot{\omega} = -\tilde{K}\rho Y e^{-\tilde{T}/T}, \quad (8)$$

where  $T$  is the temperature,  $\tilde{T}$  is the activation temperature, and  $\tilde{K}$  is a constant pre-exponential factor. For ideal gas which has the following non-dimensional equation of state:

$$p = \rho T. \quad (9)$$

### 3 Numerical Method

Structured meshes with hexahedral elements will be used here. A schematic diagram of element  $K_{\bar{i},\bar{j},\bar{k}}$  is shown in Fig.1(a). Owing to the movement of the mesh points, the hexahedron element will change into a polyhedron element. In order to calculate the element volume and the boundary external surface area, each surface of the hexahedron element is divided into two surfaces. The average over the cell  $K_{\bar{i},\bar{j},\bar{k}}$  is

$$\bar{\mathbf{w}}_{\bar{i},\bar{j},\bar{k}} = \frac{1}{|K_{\bar{i},\bar{j},\bar{k}}|} \int_{K_{\bar{i},\bar{j},\bar{k}}} \mathbf{w}_{\bar{i},\bar{j},\bar{k}} d\sigma. \quad (10)$$

Here,  $|K_{\bar{i},\bar{j},\bar{k}}|$  denotes the volume of the cell  $K_{\bar{i},\bar{j},\bar{k}}$ .

Integrating (1) over  $K_{\bar{i},\bar{j},\bar{k}}$  and rewriting, we express a semi-discrete scheme of (1) as:

$$|K_{\bar{i},\bar{j},\bar{k}}| \frac{\partial}{\partial t} \bar{\mathbf{w}}_{\bar{i},\bar{j},\bar{k}} = - \sum_l \mathcal{H} \left( \mathbf{w}_{\bar{i},\bar{j},\bar{k}}^{int(l)}, \mathbf{w}_{\bar{i},\bar{j},\bar{k}}^{ext(l)}, \mathbf{n}_{\bar{i},\bar{j},\bar{k}}^l \right) |e_{\bar{i},\bar{j},\bar{k}}^l| - |K_{\bar{i},\bar{j},\bar{k}}| \mathbf{s}(\bar{\mathbf{w}}_{\bar{i},\bar{j},\bar{k}}) \quad (11)$$

where  $\mathbf{n}_{\bar{i},\bar{j},\bar{k}}^l$  is the outward unit normal vector of the boundary external surface  $e_{\bar{i},\bar{j},\bar{k}}^l$  ( $l = 1, 2, \dots, 12$ ). And Lax-Friedrichs flux is defined by

$$\mathcal{H}(\mathbf{u}, \mathbf{v}, \mathbf{n}) = \frac{1}{2} [\mathcal{F}(\mathbf{u}) \cdot \mathbf{n} + \mathcal{F}(\mathbf{v}) \cdot \mathbf{n} - a(\mathbf{v} - \mathbf{u})], \quad (12)$$

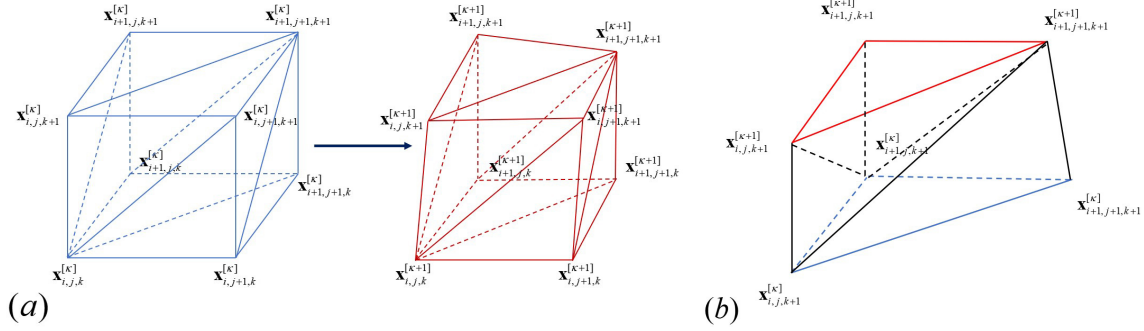


Figure 1: (a):Schematic diagram of the control element  $K_{\bar{i},\bar{j},\bar{k}}^{[k]}$ ; (b): Changed area  $D_1$

where  $a = \max_{\mathbf{u}, \mathbf{n}} |\mathcal{F}'(\mathbf{u}) \cdot \mathbf{n}|$ ,  $\mathcal{F}(\mathbf{w}) = (\mathbf{f}(\mathbf{w}), \mathbf{g}(\mathbf{w}), \mathbf{h}(\mathbf{w}))$ . In order to obtain the second-order spatial accuracy, we use van Leer's limiter [3] to reconstruct  $\mathbf{w}_{\bar{i},\bar{j},\bar{k}}^{int(l)}$ ,  $\mathbf{w}_{\bar{i},\bar{j},\bar{k}}^{ext(l)}$ . Time discretization can be achieved using the strong stability-preserving high-order Runge-Kutta time discretization [4, 5].

Next, we present the derivation of the three-dimensional pseudo-arc-length moving mesh scheme. Let  $\mathbf{x} = (x, y, z)$  and  $\xi = (\xi, \eta, \zeta)$  denote the physical and computational coordinates, respectively. A one-to-one coordinate transformation from the computational domain  $\Omega_c$  to the physical domain  $\Omega_p$  is denoted by

$$(x, y, z) = (x(\xi, \eta, \zeta), y(\xi, \eta, \zeta), z(\xi, \eta, \zeta)). \quad (13)$$

In the variational approach, the mesh map aims to find the minimizer of the functional

$$\Phi(x, y, z) = \frac{1}{2} \int_{\Omega_c} [\nabla^T x G_1 \nabla x + \nabla^T y G_2 \nabla y + \nabla^T z G_3 \nabla z] d\xi d\eta d\zeta, \quad (14)$$

where  $G_1$ ,  $G_2$ , and  $G_3$  are given symmetric positive definite matrices called monitor functions, and  $\nabla = (\partial_\xi, \partial_\eta, \partial_\zeta)^T$ . The corresponding Euler-Lagrange equation is given by

$$\begin{aligned} \partial_\xi (G_1 \partial_\xi x) + \partial_\eta (G_1 \partial_\eta x) + \partial_\zeta (G_1 \partial_\zeta x) &= 0, \\ \partial_\xi (G_2 \partial_\xi y) + \partial_\eta (G_2 \partial_\eta y) + \partial_\zeta (G_2 \partial_\zeta y) &= 0, \\ \partial_\xi (G_3 \partial_\xi z) + \partial_\eta (G_3 \partial_\eta z) + \partial_\zeta (G_3 \partial_\zeta z) &= 0. \end{aligned} \quad (15)$$

In order to make the adaptive grid keep consistent in  $x, y, z$ , we choose  $G = \omega I$ . For greater accuracy near the non-smooth part of the solutions, we introduce the monitor function of the pseudo-arc-length norm [6]:

$$\omega = \sqrt{1 + \alpha_1 |W| + \alpha_2 |\nabla W|^2}, \quad (16)$$

where  $\alpha_1$  and  $\alpha_2$  are some nonnegative constants, and  $W$  is some physical value to control mesh movement (density, pressure, etc. are commonly used). In our computations, we will use the Gauss-Seidel iteration method to solve the mesh equation (15). It can also be demonstrated that the new mesh  $\mathbf{x}^{[\kappa+1]}$  generated by (17) keeps the monotonic order of  $\mathbf{x}^{[\kappa]}$ . Because of the limit of the paper, we omit the certificate.

Then, let us consider updating of the solutions on the new grids  $\mathbf{x}^{[\kappa+1]}$  from the old grids  $\mathbf{x}^{[\kappa]}$ . Han and Tang [7] have claimed that updating of the solutions should preserve the conservation property of the conservative variables. Our schemes also preserve the conservative property for  $\bar{\mathbf{w}}_{\bar{i},\bar{j},\bar{k}}$  in the sense that:

$$\sum_{\bar{i},\bar{j},\bar{k}} |K_{\bar{i},\bar{j},\bar{k}}^{[\kappa]}| \bar{\mathbf{w}}_{\bar{i},\bar{j},\bar{k}}^{[\kappa]} = \sum_{\bar{i},\bar{j},\bar{k}} |K_{\bar{i},\bar{j},\bar{k}}^{[\kappa+1]}| \bar{\mathbf{w}}_{\bar{i},\bar{j},\bar{k}}^{[\kappa+1]}. \quad (17)$$

Let  $D_l$  denote the region scanned by the surface  $e_{i,\bar{j},\bar{k}}^l$  after one iterative step of (18). Thus, we have the following conservative interpolation scheme:

$$\left| K_{i,\bar{j},\bar{k}}^{[\kappa+1]} \right| \bar{\mathbf{w}}_{i,\bar{j},\bar{k}}^{[\kappa+1]} = \left| K_{i,\bar{j},\bar{k}}^{[\kappa]} \right| \bar{\mathbf{w}}_{i,\bar{j},\bar{k}}^{[\kappa]} + \sum_{l=1}^{12} \hat{F}_l \left( \bar{\mathbf{w}}_{i,\bar{j},\bar{k}}^{\text{int}(l)}, \bar{\mathbf{w}}_{i,\bar{j},\bar{k}}^{\text{ext}(l)} \right) \quad (18)$$

Here,  $\hat{F}_l(\cdot, \cdot)$  denotes the integration of  $\bar{\mathbf{w}}$  over the domain  $D_l$ . Then, we give an approximation of  $\hat{F}_l(\cdot, \cdot)$ :

$$\hat{F}_l(\mathbf{u}, \mathbf{v}) = \max(|D_l|, 0) \cdot \mathbf{v} + \min(|D_l|, 0) \cdot \mathbf{u}. \quad (19)$$

For example, we compute  $D_1$ . The modified area  $D_1$  is shown in Fig.1(b). Note that  $D_1$  is composed of three tetrahedrons; hence, we have

$$\begin{aligned} D_1 = & V_{\mathbf{x}_{i+1,j,k+1}^{[\kappa]} \mathbf{x}_{i+1,j,k+1}^{[\kappa+1]} \mathbf{x}_{i+1,j+1,k+1}^{[\kappa+1]} \mathbf{x}_{i,j,k+1}^{[\kappa+1]}} + V_{\mathbf{x}_{i+1,j,k+1}^{[\kappa]} \mathbf{x}_{i+1,j+1,k+1}^{[\kappa+1]} \mathbf{x}_{i,j,k+1}^{[\kappa]} \mathbf{x}_{i,j,k+1}^{[\kappa+1]}} \\ & + V_{\mathbf{x}_{i+1,j,k+1}^{[\kappa]} \mathbf{x}_{i+1,j+1,k+1}^{[\kappa+1]} \mathbf{x}_{i+1,j+1,k+1}^{[\kappa]} \mathbf{x}_{i,j,k+1}^{[\kappa]}}. \end{aligned} \quad (20)$$

#### 4 Numerical examples

Example 1. The first test problem is a spherical shock wave expanded in an enclosed box using the Euler equations without the chemical source term [8, 9]. The computational domain is  $[0, 1] \times [0, 1] \times [0, 1]$ , and divided uniformly into  $100 \times 100 \times 100$  cells. In order to improve the computational efficiency, the MPI parallel computing mode are used with a total of  $16(4 \times 2 \times 2)$  processes. All the boundaries are treated as a reflective wall. Initially, the primitive variables are set as follows:

$$(\rho, u, v, w, p) = \begin{cases} (5, 0, 0, 0, 5) & \text{for } \sqrt{(x-0.4)^2 + (y-0.4)^2 + (z-0.4)^2} \leq 0.3, \\ (1, 0, 0, 0, 1) & \text{other.} \end{cases} \quad (21)$$

The monitor function is given by  $\omega = \sqrt{1 + 100|\rho|^2 + 50|\nabla\rho|^2}$ .

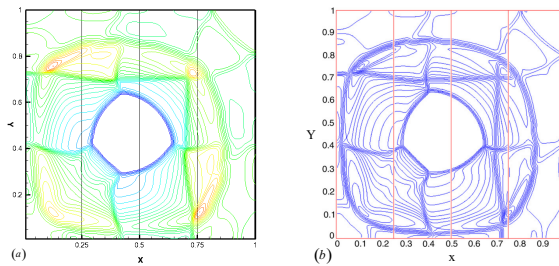


Figure 2: Density contours in  $z = 0.4$  section at time  $t = 0.5$ . (a)pseudo-arc-length schemes; (b) ref. [9].

Fig.2 shows the density contours of explosion in a box in the  $z = 0.4$  section at time  $t = 0.5$ . The density contours (density=1.8) obtained are shown in Fig.3. Fig.2(a) and Fig.3(a) show the results of our schemes. For comparison, Fig.2(b) and Fig.3(b) show the results [8, 9] which are obtained via the block-structure adaptive mesh refinement technique. In Fig.2, no significant difference can be seen between the two results.

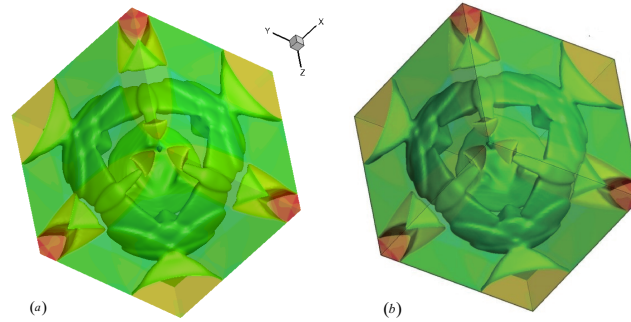


Figure 3: **Density contours (density= 1.8) at time  $t = 0.5$ . (a) pseudo-arc-length schemes; (b) ref. [8].**

Complex features, such as the shocks and the interactions between the shocks, are well captured. Clearly, the results of our schemes are in good agreement with those presented in [8, 9] (Fig.3). These two figures show that our schemes can effectively simulate three-dimensional compressible inviscid flows with complex shock wave structures, and our results are reliable.

Example 2. This is a three-dimensional detonation diffraction problem. The computational domain are shown in Fig.4. The number of computational mesh is  $N_x \times N_y \times N_z = 120 \times 80 \times 80$ . We also use the MPI parallel computing mode with a total of  $16(4 \times 2 \times 2)$  processes. The boundaries of the area in our simulation are non-reflective and the boundary conditions for the obstacle  $([0, 1] \times [0, 1] \times [0, 1])$  are reflective. Let  $(\rho, u, p, Y) = (1, 0, 1, 1)$  be the physical values of the unreacted region. The analytical solutions of the ZND model [10] are taken as the initial values for the simulation. The non-dimensional reaction parameters are taken as  $\gamma = 1.2$ ,  $Q = 50$ ,  $\tilde{T} = 50$ ,  $\tilde{K} = 230.75$ , and  $f = 1.0$ . The monitor function is given by  $\omega = \sqrt{1 + 5|\rho|^2 + 3|\nabla\rho|^2}$ . If we choose different parameters  $\alpha_1, \alpha_2$  or physical variables  $W$ , we will obtain various adaptive meshes. We will report these results at the meeting.

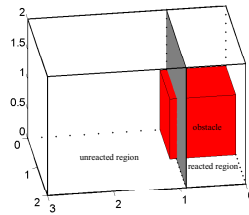


Figure 4: **Computational domain of example 2.**

Fig.5 shows the simulate solutions and mesh at time  $t = 0.2$ . From Fig.5(a) and Fig.5(b), we can see that our scheme can deal with the low-pressure and low-density region behind the obstacle. The entire adaptive mesh is shown in Fig.5(c). The slices of the mesh changing with pressure at different times are compared in Figs.6. It shows that the adaptive mesh can capture the blast wave front.

## References

- [1] Wang C, Liu XQ. (2015). High resolution numerical simulation of detonation diffraction of condensed explosives. *Int. J. Comput. Meth.* 12(02):1550005.

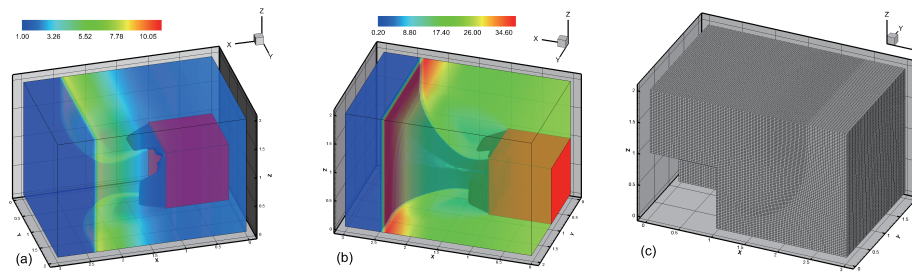


Figure 5: Contour of three-dimensional flow at time  $t = 0.2$ . (a) density ( $\rho = 0.3$ ); (b) pressure ( $p = 2.0$ ); (c) mesh.

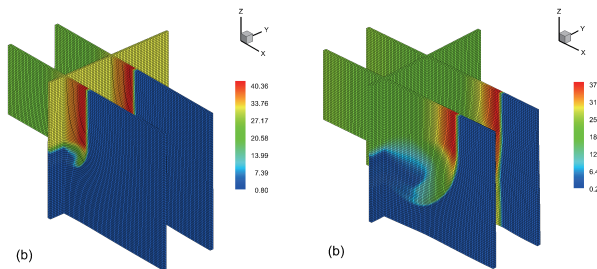


Figure 6: Slices of mesh in three-dimensional space. (a) time  $t = 0.076$ ; (b) time  $t = 0.2$ .

- [2] Ji H, Lien FS, Yee E. (2010). Numerical simulation of detonation using an adaptive Cartesian cut-cell method combined with a cell-merging technique. *Comput. Fluid.* 39(6):1041-1057.
- [3] Leer BV. (1979). Towards the ultimate conservative difference scheme. v. a second-order sequel to godunov's method. *J. Comput. Phys.* 32(1):101-136.
- [4] Shu CW, Osher S. (1988). Efficient implementation of essentially non-oscillatory shock-capturing schemes. *J. Comput. Phys.* 77(2):439-471.
- [5] Godlieb S, Shu CW. (1998). Total variation diminishing runge-kutta schemes. *Math. Comp.* 67(221):73-85.
- [6] Wang X, Ma TB, Ning JG. (2014). A pseudo arc-length method for numerical simulation of shock waves. *Chin. phys. lett.* 31(03):30201-030201.
- [7] Han J, Tang H. (2007). An adaptive moving mesh method for two-dimensional ideal magnetohydrodynamics. *J. Comput. Phys.* 220(2):791-812.
- [8] Yang LM, Shu C, Wu J. (2015). A three-dimensional explicit sphere function-based gas-kinetic flux solver for simulation of inviscid compressible flows. *J. Comput. Phys.* 295:322-339.
- [9] Deiterding R. [http://amroc.sourceforge.net/examples/euler/3d/html/box3d\\_n.htm](http://amroc.sourceforge.net/examples/euler/3d/html/box3d_n.htm).
- [10] Fickett W, Wood WW. (1966). Flow Calculations for Pulsating One-Dimensional Detonations. *Physics of Fluids.* 9(5):903-916.